# Carbonatitic melts along the solidus of model lherzolite in the system CaO-MgO-Al 2 O 3–SiO 2–CO 2 from 3 to 7 GPa

2 authors, including:

Dean. C. Presnall
University of Texas at Dallas
**63** PUBLICATIONS   **3,410** CITATIONS

SEE PROFILE

**John A. Dalton · Dean C. Presnall**

# Carbonatitic melts along the solidus of model lherzolite in the system CaO-MgO-Al$_2$O$_3$-SiO$_2$-CO$_2$ from 3 to 7 GPa

**Abstract** We have experimentally determined the solidus position of model lherzolite in the system CaO-MgO-Al$_2$O$_3$-SiO$_2$-CO$_2$ (CMAS.CO$_2$) from 3 to 7 GPa by locating isobaric invariant points where liquid coexists with olivine, orthopyroxene, clinopyroxene, garnet and carbonate. The intersection of two subsolidus reactions at the solidus involving carbonate generates two invariant points, I$_{1A}$ and I$_{2A}$, which mark the transition from CO$_2$-bearing to dolomite-bearing and dolomite-bearing to magnesite-bearing lherzolite respectively. In CMAS.CO$_2$, we find I$_{1A}$ at 2.6 GPa/1230 °C and I$_{2A}$ at 4.8 GPa/1320 °C. The variation of all phase compositions along the solidus has also been determined. In the pressure range investigated, solidus melts are carbonatitic with SiO$_2$ contents of < 6 wt%, CO$_2$ contents of ~45 wt%, and Ca/(Ca + Mg) ratios that range from 0.59 (3 GPa) to 0.45 (7 GPa); compositionally they resemble natural magnesiocarbonatites. Volcanic magnesiocarbonatites may well be an example of the eruption of such melts directly from their mantle source region as evidenced by their diatremic style of activity and lack of associated silicate magmas. Our data in the CMAS.CO$_2$ system show that in a carbonate-bearing mantle, solidus and near-solidus melts will be CO$_2$-rich and silica poor. The widespread evidence for the presence of CO$_2$ in both the oceanic and continental upper mantle implies that such low degree SiO$_2$-poor carbonatitic melts are common in the mantle, despite the rarity of carbonatites themselves at the Earth's surface.

J.A. Dalton (✉) · D.C. Presnall
Magmalogy Laboratory, Department of Geosciences,
University of Texas at Dallas, Box 830688, Richardson,
TX 75083-0688, U.S.A.
Telephone: 972-883-6396, Fax: 972-883-2537
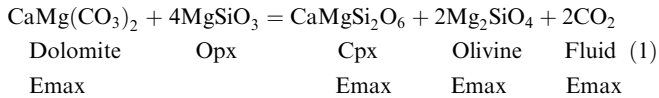E-mail: dalton@utdallas.edu

## Introduction

The realization that carbonatite magmas have an upper mantle origin prompted numerous studies of the role of CO$_2$ in mantle assemblages, primarily in the system CaO-MgO-SiO$_2$-CO$_2$ (CMS.CO$_2$) (Wyllie and Huang 1976; Wyllie 1977; Eggler 1978). These early studies indicated that initial melts from carbonated peridotite at pressures > 2.5 GPa are CO$_2$-rich ( > 40 wt% CO$_2$) and approximate carbonatites in composition. These suggestions were later confirmed by experiments in natural systems (Falloon and Green 1989; Thibault et al. 1992; Dalton and Wood 1993b) and have led to suggestions that some carbonatites represent primary melts from the Earth's upper mantle (e.g. Bailey 1989, 1993). This conclusion is, however, not universally accepted and controversy still exists as to whether carbonatites are primary melts or whether they are the end-product of differentiation (crystal fractionation or liquid immiscibility) of a carbonated silicate magma (see review by Lee and Wyllie 1994).

Equally controversial is the problem of kimberlite petrogenesis. Until quite recently it was thought that kimberlites were formed by low degree partial melting of carbonated garnet peridotite in the diamond stability field under upper mantle conditions (Eggler and Wendlandt 1979; Wyllie 1980; Canil and Scarfe 1990). However, the discovery of majoritic garnet (now pyrope + exsolved pyroxene) in kimberlitic xenoliths (Haggerty and Sautter 1990; Sautter et al. 1991) and as an inclusion in diamond (Moore and Gurney 1985), prompted some workers to suggest that kimberlites have a much deeper origin, perhaps in the transition zone of the Earth (Ringwood et al. 1992; Haggerty 1994; Girnis et al. 1995). Critical to any model of carbonatite or kimberlite petrogenesis is a knowledge of the solidus topology and near-solidus melt compositions of carbonated lherzolite (Eggler 1987a). Figure 1 shows the solidus for model lherzolite in the system CMS.CO$_2$. The most distinctive feature of the solidus is the almost iso-

baric drop in solidus temperature as carbonate becomes a solidus phase through the reaction:

$$CaMg(CO_3)_2 + 4MgSiO_3 = CaMgSi_2O_6 + 2Mg_2SiO_4 + 2CO_2$$

| Dolomite | Opx | Cpx | Olivine | Fluid (1) |
|----------|-----|-----|---------|-----------|
| Emax | | Emax | Emax | Emax |

which intersects the solidus at the invariant point $I_1$ located by Wyllie et al. (1983) to be near 2.75 GPa/ 1225 °C and by Eggler (1978) to be at 2.9 GPa/1240 °C. Dalton and Wood (1993a) showed that the carbonate involved in reaction (1) is not stoichiometric dolomite but is a solid solution between dolomite and calcite, a feature also observed by Wyllie et al. (1983). At higher pressures dolomite is replaced as the solidus carbonate by magnesite at a second invariant point $I_2$ (Fig. 1). The positions of reactions (1) and (2) on Fig. 1 are from Wyllie et al. (1983) and Brey et al. (1983) respectively, and the solidus below 3 GPa is from Eggler (1987b). The $CMS.CO_2$ solidus shown in Fig. 1 at pressures greater than $I_2$ is taken from Canil and Scarfe (1990) and we have extended this down to $I_1$.

The appearance of carbonate on the peridotite solidus at $I_1$ results in initial melts being $CO_2$-rich as discussed above. In the $CMS.CO_2$ system, Wyllie and Huang (1976) inferred that such melts would have about 45 wt% $CO_2$, less than 10 wt% dissolved silicates, and Ca/Mg ratios >1. This general composition has been confirmed by several determinations of near-solidus melt compositions in natural carbonated peridotite at pressures ≤3 GPa (Wallace and Green 1988; Thibault et al. 1992; Dalton and Wood 1993b; Sweeney 1994) but there are some differences. These primarily result from differences in choice of bulk composition and as yet there is no consensus as to the range of primary carbonate melt

compositions that can be produced from peridotite. In fact, none of these studies has produced carbonate melt in equilibrium with four phase anhydrous lherzolite. Dalton and Wood (1993b) presented data on the composition of carbonate melt in equilibrium with anhydrous harzburgite and wehrlite and suggested that carbonate melt in equilibrium with anhydrous lherzolite would be Ca-rich with a Ca/(Ca + Mg) (Ca#) ratio >0.5. In order to test models of carbonatite petrogenesis, it is imperative that the composition of carbonate melt in equilibrium with lherzolite at various pressures be obtained. This latter point is particularly important, as from Fig. 1 it is evident that the composition of the solidus carbonate changes at $I_2$ from dolomite to magnesite. It has been suggested that such a transition may also mark a change in the near-solidus melt composition with the melts becoming Mg-rich and possibly trending towards kimberlite compositions (Brey et al. 1983; Katsura and Ito 1990). However, the almost complete lack of experimental data in this pressure range has inhibited further discussion of such ideas.

In order to address these issues, we present here the melting relationships of carbonated model lherzolite in the system $CaO-MgO-Al_2O_3-SiO_2-CO_2$ ($CMAS.CO_2$) from 3 to 7 GPa. We use these data to constrain models of carbonatite and kimberlite petrogenesis.

## Experimental procedures

For a given pressure, the solidus of model carbonated lherzolite in the $CMAS.CO_2$ system corresponds to an invariant point where olivine + orthopyroxene + clinopyroxene + garnet + carbonate + liquid coexist. By determining the compositions of all the phases at such a point, it is possible, through the methods of Presnall (1986), to determine whether the point is a eutectic or peritectic and to calculate the proportion of each phase involved in the melting reaction. The advantage of this approach is that bulk compositions can be constructed that maximize the amount of liquid in the run product. As long as all six phases are present, the system remains isobarically invariant and the compositions of the phases do not change. Thus, the composition of carbonate melt in equilibrium with lherzolite can be readily analyzed by electron microprobe. As the only data in the $CMAS.CO_2$ system at pressures >3 GPa are those of Canil and Scarfe (1990), we began with a starting composition close to CCMAS1 of Canil and Scarfe (1990, Table 1) but with slightly more (4.8 wt%) $CO_2$ added. Initial experiments at 6 GPa using this composition were used to approximately locate the position of the solidus to guide further experiments and to obtain compositional information on the coexisting phases. The amount of liquid in these runs was very small and occurred interstitially but some acceptable analyses were obtained. With these data we could then construct a new bulk composition with the desired phase proportions (e.g. 40% liquid), locate the invariant point precisely with the new bulk composition, and analyze the compositions of all the phases.

Five or ten grams of each bulk composition were prepared from high purity oxides and carbonates. Carbon dioxide was added as natural magnesite (Victoria, Australia), kindly donated by Prof. D. H. Green, which contains <0.5 wt% $CaCO_3$ and <0.03 wt% $FeCO_3$ (Brey et al. 1983). The silicate portion of each starting composition was ground under methanol for 50 min and then fired for 2 h at approximately 1550 °C. The resultant glass (±crystals) was then crushed and ground for a further 50 min before the magnesite was added. The entire mixture was then ground under
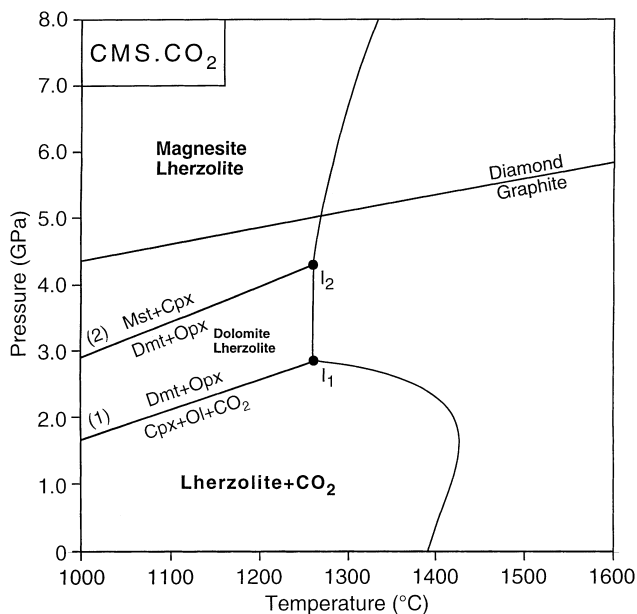


Fig. 1 Solidus curve for model carbonated lherzolite in the system $CaO-MgO-SiO_2-CO_2$ ($CMS.CO_2$). Note the sharp drop in solidus temperature as carbonate becomes a solidus phase at $I_1$

**Table 1** Experimental conditions and results

| Experiment | Pressure (GPa) | Temperature (°C) | Time (h) | Result[a] |
|---|---|---|---|---|
| KM48 | 3 | 1245 | 6 | Ol, Opx, Cpx, Gt, Dmt[b], Liq |
| KM50 | 3.5 | 1270 | 6 | Ol, Opx, Cpx, Gt, Dmt, Liq |
| KM19 | 4 | 1290 | 6 | Ol, Opx, Cpx, Gt, Dmt, Liq |
| KM25 | 5 | 1330 | 6 | Ol, Opx, Cpx, Gt, Mst, Liq |
| KM14 | 6 | 1380 | 6 | Ol, Opx, Cpx, Gt, Mst, Liq |
| KM29 | 7 | 1430 | 6 | Ol, Opx, Cpx, Gt, Mst, Liq |

[a] *Ol* olivine, *Gt* garnet, *Dmt* dolomite, *Mst* magnesite, *Liq* liquid
[b] Dmt refers to a carbonate phase that is a solid solution between $CaCO_3$ and $CaMg(CO_3)_2$

methanol for 50 min to ensure homogeneity. Approximately 1 mg of the required starting composition was loaded into a 1.2 mm O.D. platinum capsule that had previously been sealed at one end by arc-welding. The capsule plus starting composition was dried at 250 °C for at least 12 h, weighed, welded shut and weighed again. Capsules were discarded if a weight loss of $> 10\%$ (excluding capsule weight) due to decarbonation occurred during final welding. Total capsule length was 2 mm.

All experiments were performed in a multianvil apparatus at the University of Texas at Dallas. Experiments were conducted with 18 mm octahedra (95% MgO, 5% $Cr_2O_3$), WC cubes with 11 mm truncations, stepped graphite furnaces, and $Al_2O_3$ spacers and thermocouple sleeves. Temperatures were measured with W5%Re/W26%Re thermocouples positioned along the axis of the graphite heater and in contact with the Pt capsules (Fig. 2). Temperatures were automatically controlled by a Eurotherm 818 solid state controller to within $\pm 1$ °C and were uncorrected for the effect of pressure on the EMF of the thermocouple. On the basis of repeated determinations of the melting point of diopside at 2.5 and 5 GPa, temperature reproducibility is believed to be $\pm 10$ °C. Pressure calibration of the 18 mm assembly at high temperature is the same as that described by Dalton and Presnall (1997). The pressure calibration curve is linear in the pressure range 2.5–6 GPa and we have extrapolated this curve to 7 GPa where we do not expect any significant departure from linearity. Load was applied to the assembly until target pressure had been achieved and then temperature was raised at a rate of 100 °C/min. Only successful

determinations of isobaric invariant points are reported in Table 1 although many more runs were made.

## Attainment of equilibrium and hydrogen diffusion

The isobaric invariant points were not reversed and we must therefore look to other criteria to determine if our experiments approached equilibrium. Irving and Wyllie (1975) noted that reaction rates in carbonate systems at high pressures and temperatures are quite rapid with equilibrium being achieved in run times of less than 60 min. In more complex carbonate-bearing silicate systems, equilibrium has been demonstrated in run times of less than 5 h based on reversed reactions (Lee et al. 1994). Experimental durations in our experiments were in excess of these values and the high proportion of liquid in our runs is likely to facilitate equilibration. In fact, the elevated calcium content of residual olivines (Table 2) is consistent with equilibration with a Ca-rich liquid as has previously been noted for carbonate (Brenan and Watson 1991; Dalton and Wood 1993b) and silicate (Watson 1979) systems. Detailed backscattered electron imaging of the run products did not reveal any zonation in any of the phases. This suggests that equilibrium or near-equilibrium conditions were approached in our experiments.

Pyrophyllite was used as the gasket material in the multianvil runs, which opens up the possibility of hydrogen diffusion from the gaskets to the sample where it could combine with oxygen to form water. To minimize this possibility, the octahedral assembly was dried for at least 1 h at 120 °C before being immediately employed in the assembly. No evidence for $H_2$ diffusion was found in these runs in the form of hydrous phases or anomalously low melting temperatures, which suggests that our experiments were anhydrous or nearly so.
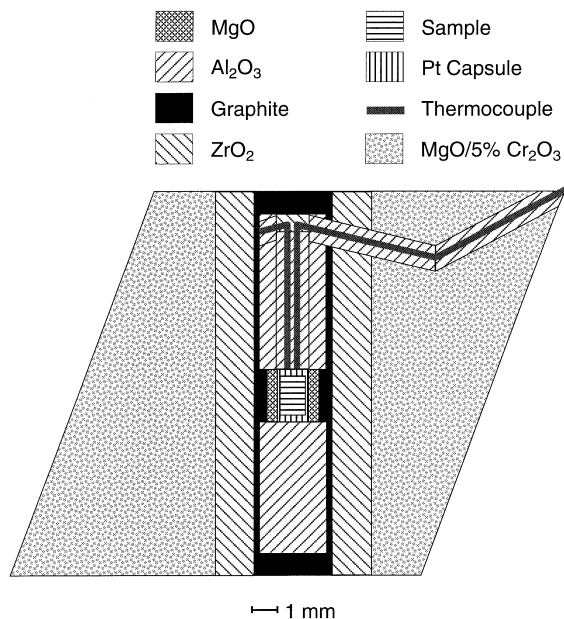
## Analytical procedures

At the conclusion of each experiment the entire capsule was mounted longitudinally in epoxy resin and ground under oil. Due to the often fragile nature of the charge, it was necessary to vacuum-impregnate the capsule repeatedly with epoxy resin and re-grind until a satisfactory surface for diamond polishing was obtained. This technique successfully minimized plucking of carbonate melt and crystalline carbonate, enabling the attainment of a flat and well polished surface necessary for electron microprobe analysis.

The compositions of the crystalline phases and of the melt were determined by wavelength dispersive electron microprobe analysis using a 5-spectrometer JEOL JXA 8600 Superprobe. The silicate phases were analyzed with a focused beam using an acceleration voltage of 15 kV and a beam current of 15 nA. Standards employed were olivine (Mg), wollastonite (Ca, Si) and garnet (Al). Data were processed using the Bence-Albee matrix correction routine with the alpha coefficients of Albee and Ray (1970). Except for garnet, at least 20 analyses of each silicate phase were made. Solid carbonate



MgO
$Al_2O_3$
Graphite
$ZrO_2$
Sample
Pt Capsule
Thermocouple
MgO/5% $Cr_2O_3$

⊢— 1 mm

**Fig. 2** Construction of the 18 mm pressure assembly used in this study

phases were analyzed according to the methodology of Lane and Dalton (1994). Briefly, carbonate standard compositions are entered into the standard file as $MO_4$ instead of $MCO_3$. ZAF calculations by means of O stoichiometry with metals of false valence 8 yield compositions as wt% oxide ($MO_4$) in the unknown carbonate, which are recalculated as metal carbonate to yield the wt% of elements in the carbonate. This method gives a total of $100\% \pm \frac{\sqrt{n}}{n}$ (where n is the number of counts and $\frac{\sqrt{n}}{n}$ is one standard deviation error due to X-ray generation statistics) which provides an indicator of analytical quality. Beam conditions were 15 kV and 5 nA for acceleration voltage and beam current respectively. For magnesian carbonates it was found that a 5 μm beam gave good analyses while for the calcium-bearing carbonates a broader beam was used where possible. Standards employed were calcite (Ca) and magnesite (Mg), the data being processed using the ZAF matrix correction routine. At least five analyses of the carbonate phase in each run were obtained.

Carbonate melt is problematical to analyze for two reasons. First, it is beam-sensitive and does not quench to a glass; therefore a defocused beam must be used. Second, the quenched matrix is dominantly composed of Ca-Mg carbonates but also contains a small silicate fraction. Thus, a representative analysis of such a melt cannot be quantitatively obtained with either of the two analytical procedures outlined above, because in each case information concerning elements present in the melt is missing from the correction routine(s). However, it is common practice to analyze carbonate melts using the same routine as for analyzing silicates. Low totals (50–60 wt%) result because $CO_2$ is not included in the correction routine. Although it is not an ideal procedure to assume $CO_2$ by difference, this is currently the most satisfactory method available and accordingly we have analyzed our melts this way. Consistency in analytical totals was achieved when analyzing the melt with all totals falling at 55 ± 1 wt%. The melt was analyzed with a 15–20 μm beam using Bence-Albee matrix correction procedures. For each experiment, 5–10 analyses of the melt were obtained.

# Experimental results

## General observations

Experiments that produced well-crystallized assemblages of olivine + orthopyroxene + clinopyroxene + garnet + carbonate, together with analyzable amounts of liquid, are considered successful determinations of isobaric invariant points. Tables 2 and 3 give the compositions of the phases at each invariant point. In the pressure range investigated (3–7 GPa), the solidus melts are $CO_2$-rich ($>40$ wt%) and $SiO_2$-poor ($\leq 6$ wt%), and can be considered carbonatitic in composition (Table 3).

In all cases, quench liquid occurs both interstitially and as a separated volume located at the top of the charge. Occasionally, separated liquid is also found at the bottom of the charge. This indicates that the temperature profile in the furnace is slightly saddle-shaped with a shallow thermal minimum in the center of the charge. Positioning of the capsule from run to run varies slightly, which accounts for the observed differences in liquid positioning from experiment to experiment. The texture of the liquid separated from the crystals is typical of carbonate melt in experimental products (e.g. White and Wyllie 1992; Dalton and Wood 1993b; Sweeney 1994) with acicular and often feathery quench carbonate interwoven with subordinate amounts of rod-like quench silicate (Fig. 3a, b). Melt that occurs interstitially has a similar type of texture except that the amount of

**Table 2** Composition of silicate phases

| Run<br>P (GPa)/T ( °C) | KM48<br>3/1245 | KM50<br>3.5/1270 | KM19<br>4/1290 | KM25<br>5/1330 | KM14<br>6/1380 | KM29<br>7/1430 |
|---|---|---|---|---|---|---|
| *Clinopyroxene* | | | | | | |
| CaO | 21.08 (38)[a] | 20.86 (50) | 23.37 (79) | 24.00 (69) | 23.32 (70) | 22.59 (62) |
| MgO | 20.50 (48) | 21.21 (38) | 19.61 (82) | 19.00 (45) | 19.56 (73) | 20.26 (52) |
| $Al_2O_3$ | 4.12 (54) | 3.19 (45) | 2.31 (50) | 2.49 (49) | 1.90 (44) | 0.78 (10) |
| $SiO_2$ | 54.12 (39) | 55.11 (44) | 54.52 (62) | 54.24 (47) | 54.77 (66) | 56.07 (35) |
| Total | 99.82 | 100.37 | 99.81 | 99.73 | 99.55 | 99.70 |
| *Orthopyroxene* | | | | | | |
| CaO | 1.85(30) | 2.44 (56) | 2.19 (33) | 1.65 (17) | 1.81 (39) | 1.80(20) |
| MgO | 36.76(41) | 36.60 (29) | 36.92 51) | 37.97 (48) | 37.79 (51) | 37.82(45) |
| $Al_2O_3$ | 4.01(29) | 3.66 (32) | 2.46 (44) | 1.12 (29) | 1.05 (14) | 0.95(11) |
| $SiO_2$ | 57.62(41) | 57.26 (68) | 58.98 (52) | 59.39 (52) | 59.66 (43) | 59.81(48) |
| Total | 100.24 | 99.96 | 100.55 | 100.13 | 100.31 | 100.38 |
| *Olivine* | | | | | | |
| CaO | 0.24(3) | 0.30 (8) | 0.25 (40) | 0.12 (5) | 0.19 (11) | 0.20(5) |
| MgO | 56.82(36) | 56.77 (36) | 56.64 (40) | 57.00 (65) | 56.49 (42) | 56.10(59) |
| $Al_2O_3$ | 0.04(3) | 0.06 (6) | 0.03 (4) | 0.01 (1) | 0.03 (3) | 0.04(2) |
| $SiO_2$ | 43.36(23) | 43.18 (40) | 43.37 (39) | 43.31 (41) | 43.34 (31) | 43.53(18) |
| Total | 100.46 | 100.31 | 100.29 | 100.44 | 100.05 | 99.87 |
| *Garnet* | | | | | | |
| CaO | 6.47(66) | 7.00 (43) | 8.80 (65) | 8.19 (31) | 8.25 (39) | 8.70(13) |
| MgO | 24.95(46) | 24.19 (35) | 23.18 (60) | 24.14 (37) | 23.77 (36) | 23.12(17) |
| $Al_2O_3$ | 24.60(34) | 24.37 (28) | 24.75 (38) | 24.12 (32) | 23.91 (30) | 23.89(12) |
| $SiO_2$ | 44.27(47) | 44.95 (30) | 43.54 (59) | 44.08 (32) | 44.22 (32) | 45.26(24) |
| Total | 100.29 | 100.51 | 100.27 | 100.54 | 100.15 | 100.97 |

[a] Value in parentheses is one standard deviation in terms of least significant digits based on at least 20 spot analyses for cpx, opx, and olivine, and at least 5 spot analyses for garnet

**Table 3** Composition of carbonate and liquid

| Run | KM48 | KM50 | KM19 | KM25 | KM14 | KM29 |
|---|---|---|---|---|---|---|
| $P$ (GPa)/$T$ (°C) | 3/1245 | 3.5/1270 | 4/1290 | 5/1330 | 6/1380 | 7/1430 |
| *Carbonate* | *Dolomite* | *Dolomite* | *Dolomite* | *Magnesite* | *Magnesite* | *Magnesite* |
| $CaCO_3$ | 72.30 (80)[a] | 67.69 (1.2) | 62.51 (98) | 10.12 (30) | 8.17 (20) | 6.42 (22) |
| $MgCO_3$ | 28.27 (70) | 31.83 (1.0) | 38.02 (70) | 90.54 (25) | 91.46 (24) | 93.61 (25) |
| Total | 100.57 | 99.52 | 100.53 | 100.66 | 99.63 | 100.03 |
| Ca/(Ca + Mg) | 0.68 (3) | 0.64 (4) | 0.58 (4) | 0.09 (4) | 0.07 (4) | 0.05 (6) |
| *Liquid* | | | | | | |
| CaO | 33.44 (26) | 31.55 (28) | 30.76 (88) | 29.11 (65) | 28.03 (89) | 25.94 (80) |
| MgO | 16.63 (20) | 17.82 (25) | 18.70 (73) | 20.24 (50) | 20.91 (1.3) | 23.26 (1.1) |
| $Al_2O_3$ | 0.64 (5) | 0.85 (5) | 0.64 (14) | 0.55 (10) | 0.66 (12) | 0.31 (4) |
| $SiO_2$ | 5.44 (24) | 6.08 (28) | 5.22 (82) | 5.36 (80) | 5.79 (93) | 5.17 (1.1) |
| $CO_2$[b] | 43.85 | 43.70 | 44.68 | 44.74 | 44.61 | 45.32 |
| Total | 100.00 | 100.00 | 100.00 | 100.00 | 100.00 | 100.00 |
| Ca/(Ca + Mg) | 0.59 (1) | 0.56 (1) | 0.54 (3) | 0.51 (3) | 0.49 (5) | 0.45 (3) |

[a] Value in parentheses is one standard deviation in terms of least significant digits based on at least 5 analyses for both carbonate and liquid
[b] By difference

the quench silicate component is lower, which may indicate quench modification of the liquid. To avoid this problem, analyses of quench liquid presented in Table 3 are all from the top of the capsule well away from the crystals.

The silicate phases always display subhedral to euhedral forms. Orthopyroxene (opx) is by far the largest phase present in experiments at pressures ≥4 GPa, frequently attaining sizes of 100 μm or more in length. In the lower pressure experiments (3 and 3.5 GPa), opx is still tabular in form but is generally ≤25 μm in size. Tiny (<5 μm), rounded inclusions of garnet, clinopyroxene, and carbonate are commonly observed in orthopyroxene. Olivines generally contain fewer inclusions and rarely attain sizes greater than 40 μm. Garnet and clinopyroxene are always the smallest of the silicate phases present with the former displaying a rounded subhedral form and sizes of 10 μm or less. Clinopyroxene (cpx) on the other hand, is usually 10–15 μm in size and almost always displays good euhedral form. Analysis of cpx in experiments KM14, 19, and 25 occasionally gave compositions distinctly different from the mean cpx analysis presented in Table 2. In particular, the Ca/Mg ratio and $Al_2O_3$ contents of these cpx are consistently lower than the dominant cpx compositions although they are indistinguishable in terms of form. These cpx display good stoichiometry, which rules out a spatial averaging effect during electron microprobe analysis, i.e. the primary excitation volume is located entirely within the cpx and not infringing on melt or other crystals below the cpx grain. Currently, we believe that these minority cpx, which account for less than 20% of the total number of cpx analyzed, are metastable cpx that formed while temperature was being raised to the final run conditions.

Carbonate in the experiments is either magnesite (5, 6 and 7 GPa), dolomite (4 GPa) or magnesian calcite (3.5 and 3 GPa) (Table 3). Magnesite typically forms subhedral to slightly rounded crystals 15–20 μm in di-
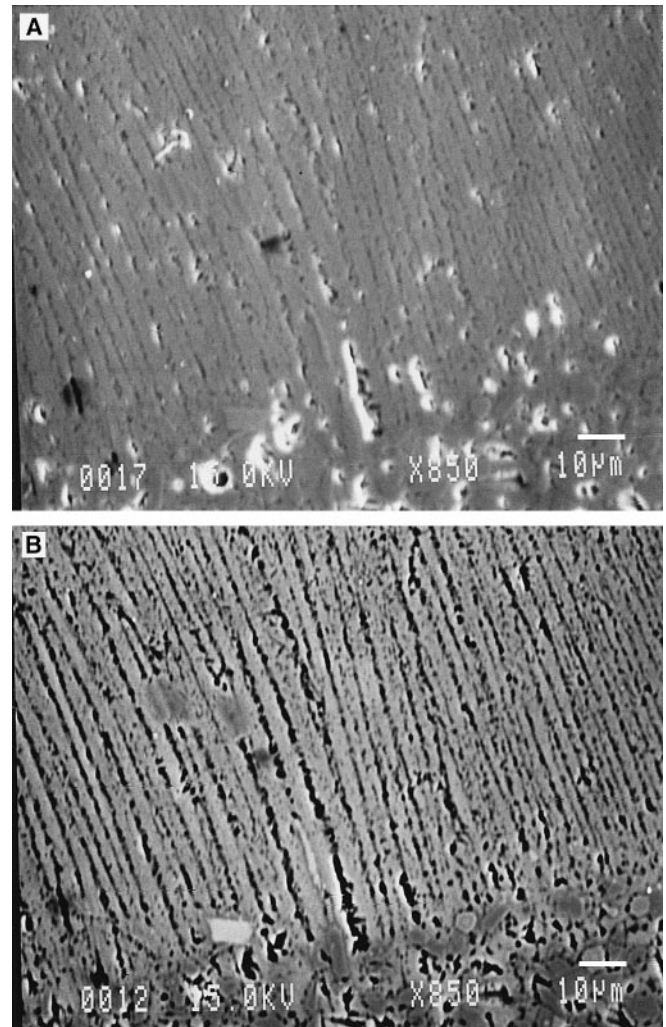
**Fig. 3A, B** Secondary electron (**A**) and backscattered electron (**B**) micrographs of the separated liquid region in experiment KM25 (5 GPa/1330 °C). Beam conditions were 15 kV and 15 nA. Note the distinctive carbonate melt quench texture in (b) and the boundary between melt and residual crystals at the base of the micrograph

ameter while dolomite occurs in a more elongated, subhedral form commonly 20–25 μm in length. It can be seen from Table 3 that the magnesite contains appreciable amounts of Ca in solid solution. Also, the calcium content of magnesite decreases linearly with increasing pressure from 5 to 7 GPa in agreement with the observations of Brey et al. (1983), who bracketed the position of reaction (2) (Fig. 1). Dolomite at 4 GPa has a Ca# of 0.58 and is thus slightly enriched in Ca with respect to stoichiometric dolomite. With decreasing pressure from 4 GPa, the calcium content of the solidus carbonate increases such that at 3.5 and 3 GPa, it is best described as magnesian calcite. However, in Table 1 and Fig. 1 and all subsequent tables and figures we have, for simplicity, retained the term dolomite to describe the carbonate phase that occurs between and including $I_1$ and $I_2$ on the carbonated lherzolite solidus even though the carbonate is a solid solution between $CaCO_3$ and $CaMg(CO_3)_2$. Magnesian calcite in KM50 (3.5 GPa) and KM48 (3 GPa) is frequently small (< 5 μm) and sometimes difficult to distinguish from the carbonate component of quench interstitial liquid. However, occasional grains ≥10 μm in size were analyzable and from Table 3 we have Ca# of 0.64 and 0.68 for 3.5 and 3 GPa, respectively. The calcitic nature of carbonate in peridotitic compositions in the 2–3 GPa pressure range has been noted by previous workers (Wyllie et al. 1983; Dalton and Wood 1993b) and our data support the conclusion that magnesian calcite is a

stable carbonate phase at upper mantle pressures and temperatures. The Ca# of 0.68 for carbonate at 3 GPa (KM48) is in good agreement with values of 0.68–0.7 reported by Dalton and Wood (1993b) for carbonate in equilibrium with olivine, opx, spinel and liquid at 3 GPa and 1300 °C.

Tables 2 and 3 give the compositions of all of the phases at each isobaric invariant point. These data are used to determine the melting reaction at each such point (Table 4) following the procedure of Presnall (1986). It can be seen that for each pressure investigated, invariant points correspond to peritectics. In the magnesite stability field (5, 6 and 7 GPa), Table 4 shows that the melting reaction changes from 6 to 7 GPa with garnet moving from the right hand side to the left hand side of the melting reaction. This indicates the occurrence of a singular point at some pressure between 6 and 7 GPa. The compositional data in Tables 2 and 3 can also be used to determine the univariant reactions and reaction coefficients about the invariant points $I_1$ and $I_2$ for the $CMAS.CO_2$ system and these are given in Table 5. To avoid confusion with the $CMS.CO_2$ system, we have termed the invariant points $I_1$ and $I_2$, $I_{1A}$ and $I_{2A}$ respectively in $CMAS.CO_2$ (Fig. 4). A comparison of Tables 4 and 5 reveals that there must be two singular points on the carbonated lherzolite solidus between $I_{1A}$ and $I_{2A}$. The first of these occurs between $I_{1A}$ and 3 GPa as garnet moves from the right hand side of the lherzolite solidus reaction at $I_{1A}$ ($CO_2$-free reaction in

**Table 4** Melting reactions

| Pressure (GPa) | Reaction[a] |
|---|---|
| 7 | *45* Mst + *0.5* Gt + *54.5* Cpx = *5* Ol + *44* Opx + *51* Liq |
| 6 | *44* Mst + *56* Cpx = *7* Ol + *40* Opx + *1* Gt + *51* Liq |
| 5 | *45* Mst + *55* Cpx = *7* Ol + *39* Opx + *3* Gt + *51* Liq |
| 4 | *76* Dmt + *23* Opx + *1* Gt = *10* Ol + *10* Cpx + *80* Liq |
| 3.5 | *68* Dmt + *32* Opx + *0.1* Gt = *10* Ol + *18* Cpx + *72* Liq |
| 3 | *69* Dmt + *31* Opx + *0.1* Gt = *8* Ol + *19* Cpx + *73* Liq |

[a] *Ol* olivine, *Gt* garnet, *Dmt* dolomite, *Mst* magnesite, *Liq* liquid

**Table 5** Univariant lines about the invariant points $I_{1A}$ and $I_{2A}$ in $CMAS.CO_2$

| | Reaction[a] |
|---|---|
| $I_{1A}$ (2.6 GPa) | *64* Dmt + *36* Opx = *10* Ol + *22* Cpx + *2* Gt + *66* Liq $(CO_2)$[b] |
| | *78* Opx + *22* Dmt = *36* Ol + *49* Cpx + *5* Gt + *10* $CO_2$ (Liq) |
| | *7* $CO_2$ + *12* Ol + *4* Cpx + *76* Dmt = *4* Opx + *96* Liq (Gt) |
| | *7* $CO_2$ + *10* Ol + *2* Opx + *80* Dmt = *0.002* Gt + *100* Liq (Opx) |
| | *7* $CO_2$ + *8* Ol + *3* Opx + *81* Dmt = *0.004* Gt + *100* Liq (Cpx) |
| | *4* $CO_2$ + *20* Opx + *76* Dmt = *11* Cpx + *1* Gt + *88* Liq (Ol) |
| | *37* Ol + *47* Cpx + *4* Gt + *12* $CO_2$ = *74* Opx + *26* Liq (Dmt) |
| $I_{2A}$ (4.8 GPa) | *84* Dmt + *11* Opx + *4* Cpx + *1* Gt = *11* Ol + *89* Liq (Mst) |
| | *52* Dmt + *28* Cpx + *20* Mst = *10* Ol + *11* Opx + *78* Liq (Gt) |
| | *55* Cpx + *45* Mst = *49* Dmt + *1* Ol + *48* Opx + *2* Gt (Liq) |
| | *72* Dmt + *17* Cpx + *11* Mst + *1* Gt = *11* Ol + *89* Liq (Opx) |
| | *84* Dmt + *1* Gt + *15* Opx = *11* Ol + *86* Liq + *3* Mst (Cpx) |
| | *53* Dmt + *2* Gt + *45* Opx = *50* Cpx + *42* Mst + *9* Liq (Ol) |
| | *56* Cpx + *44* Mst = *7* Ol + *1* Gt + *40* Opx + *51* Liq (Dmt) |

[a] Phase abbreviations as in Table 4
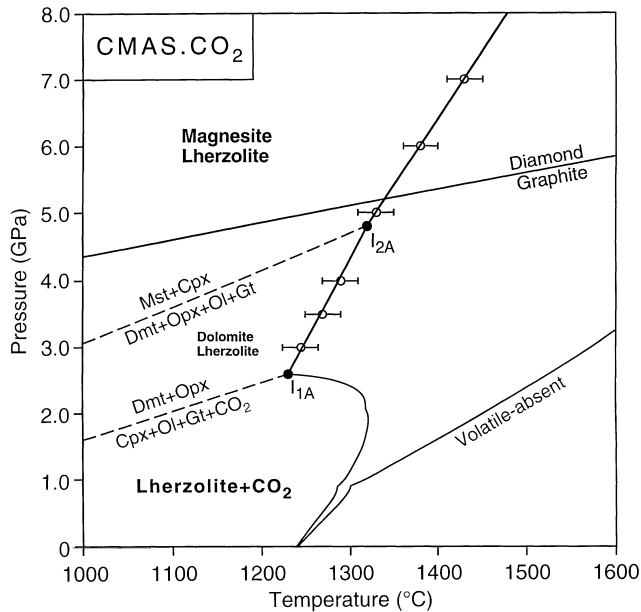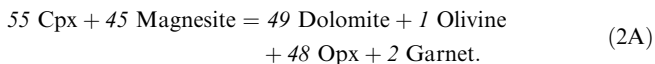[b] Absent phase in parentheses

**Fig. 4** Solidus curve for model carbonated lherzolite (Ol + Opx + Cpx + Gt + carbonate) in the system CaO-MgO-Al$_2$O$_3$-SiO$_2$-CO$_2$ (CMAS.CO$_2$) determined in this study. The volatile-absent lherzolite solidus in the CMAS system is from Gudfinnsson and Presnall (1996)

Table 5), to the left hand side of the solidus reaction at 3 GPa as seen in Table 4. The second singular point occurs between 4 and 4.8 GPa (I$_{2A}$) where cpx moves from the right hand side of the lherzolite solidus reaction at 4 GPa (Table 4), to the left hand side of the solidus reaction at I$_{2A}$ (magnesite-free reaction, Table 5).

It is also evident from Table 5 that the two sub-solidus, liquid-absent reactions in the CMAS.CO$_2$ system which terminate at I$_{1A}$ and I$_{2A}$ are not identical to the liquid-absent reactions in the CMS.CO$_2$ system, reactions (1) and (2), which terminate at I$_1$ and I$_2$ respectively on Fig. 1. In the Al-bearing system, the liquid-absent reaction that introduces dolomite as a solidus phase at I$_{1A}$ is:

$$78 \text{ Opx} + 22 \text{ Dolomite} = 36 \text{ Olivine} + 49 \text{ Cpx} \\ + 5 \text{ Garnet} + 10 \text{ CO}_2 \qquad (1A)$$
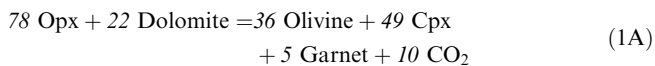
while the liquid-absent reaction that marks the change from dolomite-bearing to magnesite-bearing lherzolite at I$_{2A}$ is:

$$55 \text{ Cpx} + 45 \text{ Magnesite} = 49 \text{ Dolomite} + 1 \text{ Olivine} \\ + 48 \text{ Opx} + 2 \text{ Garnet.} \qquad (2A)$$

We have labeled these reactions 1A and 2A to distinguish them from the liquid-absent reactions in the CMS.CO$_2$ system (Fig. 1). Brey et al. (1983) determined the position of reaction (2) in the CMS.CO$_2$ system using both piston-cylinder (to 4 GPa) and belt apparatus (to 5 GPa). In Fig. 1 we show only their piston-cylinder determination in order to be consistent with Wyllie et al. (1983), who located reaction (1) in a piston-

cylinder apparatus. From the phase compositions in Table 1 of Brey et al. (1983) we can calculate coefficients for reaction (2) in the CMS.CO$_2$ system:

$$56 \text{ Cpx} + 44 \text{ Magnesite} = 48 \text{ Dolomite} + 52 \text{ Opx.}$$
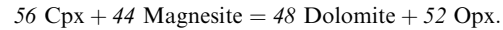
For the purposes of this calculation we have assumed that olivine is not involved in this reaction although this may not strictly be the case if olivine contains a small amount of CaO. The good agreement in reaction coefficients between reactions (2) and (2A) is encouraging, and implies that the two reactions are not far apart in *PT* space. This is because the compositions of diopside, enstatite, dolomite, and magnesite are sensitive to changes in *P* and/or *T* (Brey et al. 1983; this study), and thus one would expect to see very different reaction coefficients for (2) and (2A) if they were in very different *PT* positions. Reactions (1A) and (2A) are more representative of the natural situation than reactions (1) and (2).

## Lherzolite solidus in the CMAS.CO$_2$ system

Figure 4 shows the position of the carbonated lherzolite solidus in the CMAS.CO$_2$ system from 3 to 7 GPa determined in this study. In agreement with Canil and Scarfe (1990), we find that the essential topology of the corresponding solidus in the CMS.CO$_2$ system is retained when Al$_2$O$_3$ is added to the system. The d$T$/d$P$ slope of the CMAS.CO$_2$ solidus is approximately the same as that for the temperature minimum on the solidus and liquidus between calcite and dolomite, the latter being some 30–40 °C higher in the 3–6 GPa pressure range (Irving and Wyllie 1975). This confirms the suggestion of Wyllie (1977) that the carbonated lherzolite solidus at pressures above I$_1$ would have a d$T$/d$P$ slope parallel to the carbonate fusion curves and illustrates the strong control of the temperature minimum in the CaCO$_3$-CaMg(CO$_3$)$_2$ system on the solidus temperature in CO$_2$-bearing peridotite systems (Wyllie and Huang 1976). We show the volatile-absent CMAS solidus on Fig. 4 (Gudfinnsson and Presnall 1996) to emphasize the large difference in temperature between the volatile-absent and volatile-bearing solidi at pressures > 2 GPa. Although we have no data on the location of the CMAS.CO$_2$ solidus at pressures below I$_{1A}$, its position is constrained to be at lower temperatures than the volatile-absent solidus. With decreasing pressure, the two solidi approach each other as the solubility of CO$_2$ in silicate melt becomes lower with decreasing pressure (Mysen 1975) until at 1 atm (0.101 MPa) the two curves will be at effectively the same temperature. The low-temperature cusp in both of these solidi at a pressure of approximately 0.9 GPa results from the intersection of the subsolidus spinel lherzolite to plagioclase lherzolite transition with the solidus. Likewise the intersection of the spinel lherzolite to garnet lherzolite transition with the solidus also generates a cusp on the CMAS.CO$_2$ solidus at approximately 2.1 GPa (Fig. 4).

In the preceding section it was made clear that the two liquid-absent reactions in the $CMAS.CO_2$ system, (1A) and (2A), are not equivalent to reactions (1) and (2) in the $CMS.CO_2$ system shown on Fig. 1. The involvement of small amounts of garnet in reaction (1A) and both garnet and olivine in reaction (2A), requires that these two reactions have differing $PT$ coordinates to reactions (1) and (2) respectively. However, we have no data on the position of these reactions, nor is it possible to calculate their position for pure phases and then adjust for non-ideality, because there is no other aluminous phase to balance garnet in either of these reactions. Thus, until experimental data become available, we have recalculated the positions of reactions (1) and (2) to include the effect of solid solution on these reactions based on our data in the $CMAS.CO_2$ system (Tables 2 and 3) and the equations of Dalton and Wood (1993a) and we show these as dashed lines in Fig. 4. For these calculations, olivine and garnet, although present in small amounts, have been ignored. With these approximate positions for curves (1A) and (2A), we obtain approximate positions for the two invariant points $I_{1A}$ and $I_{2A}$ for the $CMAS.CO_2$ system at 2.6 GPa/1230 °C and 4.8 GPa/1320 °C, respectively (Fig. 4). In accordance with Schreinemakers' rules we show a slight change in the slope of the $CMAS.CO_2$ solidus at $I_{2A}$ where the sub-solidus reaction intersects the solidus. The location of $I_{2A}$ is supported by our experiments that show magnesite as the stable carbonate phase in equilibrium with lherzolite at the solidus at 5 GPa, and dolomite as the stable carbonate phase at the lherzolite solidus at 4 GPa (Table 1). These runs bracket the intersection of reaction (2A) with the solidus (i.e. $I_{2A}$) between 4 and 5 GPa. We do not have the same level of constraint on the location of reaction (1A) but it is unlikely that the addition of a small amount of garnet to this reaction would shift its position significantly.

White and Wyllie (1992) recently presented data for the $CMS.CO_2$ system and show $I_1$ to be close to 2.87 GPa and 1265 °C (Fig. 3, White and Wyllie 1992). This position is consistent with the data of Eggler (1978) on the position of the $CMS.CO_2$ solidus at pressures $>I_1$, and with the Wyllie et al. (1983) position of reaction (1) in the $CMS.CO_2$ system. Our determination of $I_{1A}$ in $CMAS.CO_2$ at 2.6 GPa/1230 °C is also consistent with a location for $I_1$ in $CMS.CO_2$ at between 2.8 and 2.9 GPa and 1260–1270 °C, i.e. at slightly higher pressure and temperature than in the $CMAS.CO_2$ system. Furthermore, the ~30 °C difference between $I_1$ in $CMS.CO_2$ and $I_{1A}$ in $CMAS.CO_2$ is in good agreement with the observed 50 °C difference between the $CMAS.CO_2$ solidus (data from this study) and the $CMS.CO_2$ solidus at 7 GPa (Arima and Presnall, work in preparation).

Figure 5 compares our determination of the $CMAS.CO_2$ solidus together with the $CMS.CO_2$ and $CMAS.CO_2$ solidi of Canil and Scarfe (1990). Note that our solidus occurs at much higher temperatures than either the $CMS.CO_2$ or the $CMAS.CO_2$ solidus of Canil

and Scarfe (1990). In fact, our solidus is consistently about 100 °C higher than the $CMAS.CO_2$ solidus of Canil and Scarfe (1990) but has essentially the same slope. We have no certain explanation for this discrepancy or for the observation that the $CMS.CO_2$ and $CMAS.CO_2$ solidi of Canil and Scarfe (1990) cross at a pressure of approximately 6.65 GPa (Fig. 5). However, in the pressure assembly employed by Canil and Scarfe (1990), the thermocouple is inserted through the side of the heater. As discussed by Herzberg et al. (1990), a thermocouple inserted in this manner will read melting temperatures that are too low. From our data and that of Arima and Presnall (in preparation), the estimated position of the $CMS.CO_2$ solidus at pressures above $I_1$ is shown as a dashed line in Fig. 5 together with reactions (1) and (2) in $CMS.CO_2$ and the solidus below $I_1$ (all from Fig. 1). From Fig. 5 it can be seen that the width of the solidus ledge is less in $CMAS.CO_2$ than in $CMS.CO_2$. It should be noted, however, that as we have no data on the position of the $CMAS.CO_2$ solidus below $I_{1A}$, the ledge could be broader than shown in Figs. 4 and 5, although it will always occur at a lower temperature than the $CMS.CO_2$ solidus.

Composition of carbonate melts

Table 3 shows that solidus melt compositions are carbonatitic in nature with high $CO_2$ and low $SiO_2$ con-
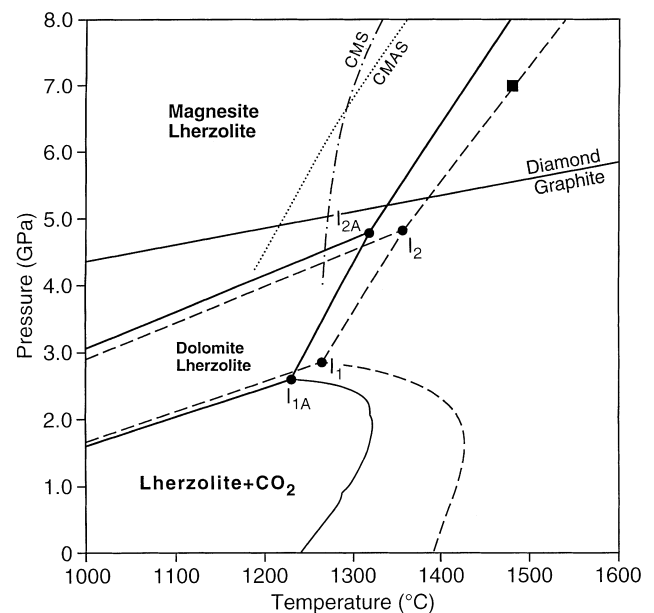


**Fig. 5** Comparison of the carbonated lherzolite solidus in the $CMAS.CO_2$ system determined in this study with the carbonated lherzolite solidi in the $CMS.CO_2$ (*dash-dot*) and $CMAS.CO_2$ (*dotted*) systems determined by Canil and Scarfe (1990) from 4 to 12 GPa. Also shown by the *filled square* is the position of the carbonated lherzolite solidus in the $CMS.CO_2$ system at 7 GPa determined by Arima and Presnall (in preparation), and the $CMS.CO_2$ solidus and decarbonation reactions from Fig. 1 together with the estimated position of the solidus above $I_1$ (all *dashed lines*)

tents, neither of which shows any significant variation in the pressure range investigated. However, the Ca and Mg contents of both the carbonate melt and coexisting crystalline carbonate change along the solidus and this is shown in Fig. 6 as a plot of Ca# against pressure.

### Solidus melts in the magnesite stability field

Figure 6 and Table 3 show that carbonate melt compositions in the magnesite stability field are dolomitic in character with Ca/(Ca + Mg) ratios of 0.45, 0.49, and 0.51 for 7, 6, and 5 GPa, respectively. The coexisting magnesite in these experiments shows a substantial Ca content in this pressure range that systematically decreases with increasing pressure along the solidus (Fig. 6). This is reflected in the Ca content of the coexisting carbonate melt, which likewise shows a decrease in Ca content with increasing pressure from 5 to 7 GPa. However, the Mg/Ca ratios of these melts (0.96–1.4) are still lower than those determined for natural kimberlites ($>2.5$), which argues against a transition in solidus melt composition from carbonatitic to kimberlitic-like melts with increasing pressure, certainly to 7 GPa. Thus, the presence of magnesite rather than dolomite as the stable carbonate phase does not lead to a significant increase in the Mg content of the melt as has been suggested (Brey et al. 1983; Katsura and Ito 1990). It is also noteworthy that the $SiO_2$ and $CO_2$ contents of the melts in the magnesite stability field are indistinguishable from those in the dolomite stability field (Table 3). This implies that as long as carbonate is a stable phase in mantle assemblages, solidus melts will always be $CO_2$-rich and $SiO_2$-poor, even at pressures significantly higher than the maximum achieved in our data set. Such carbonate melts may be important in pre-enriching the source region(s) of both kimberlites and carbonatites, but the

relationship of these melts to primary kimberlite melts, if they exist, remains uncertain.

### Solidus melts in the dolomite stability field

As pressure decreases from 4.8 GPa at $I_{2A}$, the carbonate melt and coexisting carbonate trend towards increasingly calcitic compositions. It has already been noted that carbonate compositions at 3.5 (Ca#, 0.64) and 3 GPa (Ca#, 0.68) are magnesian calcite in composition (Table 3). Dalton and Wood (1993a) showed that at temperatures exceeding the crest of the calcite-dolomite solvus ($\sim1020\,°C$ at 3 GPa), the carbonate involved in reaction (1) is disordered and is a solid solution between calcite and dolomite. They distinguished a field of carbonate solid solution at temperatures above the solvus crest and pressures above reaction (1) but below reaction (2), where the carbonate becomes more magnesian (i.e. closer to dolomite) with increasing pressure. The carbonate data presented in Fig. 6 confirm this trend and indicate that the Ca# of dolomite at $I_{2A}$ would be $\sim0.5$ and that of magnesian calcite at $I_{1A}$ would be $\sim0.72$, in good agreement with the experimental data of Brey et al. (1983) and Wyllie et al. (1983) respectively in $CMS.CO_2$. The experimental demonstration that magnesian calcite is stable in lherzolitic assemblages is supported by the recent finding of magnesian calcite in lherzolitic xenoliths from Spitsbergen (Ionov et al. 1996).

Wyllie (1977) and Eggler (1978) suggested from phase relations in $CMS.CO_2$ that near solidus carbonate melts at pressures at and just above $I_1$ would have Ca# $>0.5$. Our present data at 3.5 (Ca#, 0.56) and 3 GPa (Ca#, 0.59) in $CMAS.CO_2$ confirm these earlier suggestions that the composition of carbonate melt in equilibrium with carbonated model lherzolite in $CMS.CO_2$ and $CMAS.CO_2$ at pressures at and just above $I_1/I_{1A}$ is not dolomitic, but is enriched in calcium relative to dolomite (Table 3; Fig. 6). However, the Ca# of the carbonate melt at 3 GPa determined in this study is less than the value of 0.68 given by Dalton and Wood (1993b) for carbonate melt in equilibrium with natural harzburgite at the equivalent pressure. To resolve this discrepancy, we repeated the 3 GPa experiment of Dalton and Wood (1993b) using the same starting composition (SM57) except that more cpx was added to ensure cpx saturation. Analyses of the separated liquid phase at 3 GPa and 1250 °C in which olivine, cpx, opx and carbonate were present, gives a Ca# of 0.57 with the $SiO_2$ content of the melt ranging from 5 to 8.5 wt%. These values are in excellent agreement with the current data for $CMAS.CO_2$ at 3 GPa. Compared to the separated liquid, the $SiO_2$ content of the interstitial liquid in this run is generally lower ($<3$ wt%) and the Ca# is higher, with values up to 0.69, i.e. the liquids are compositionally similar to those reported by Dalton and Wood (1993b). In fact, a similar pattern emerges from analyses of interstitial liquid in the $CMAS.CO_2$ runs. For example, a
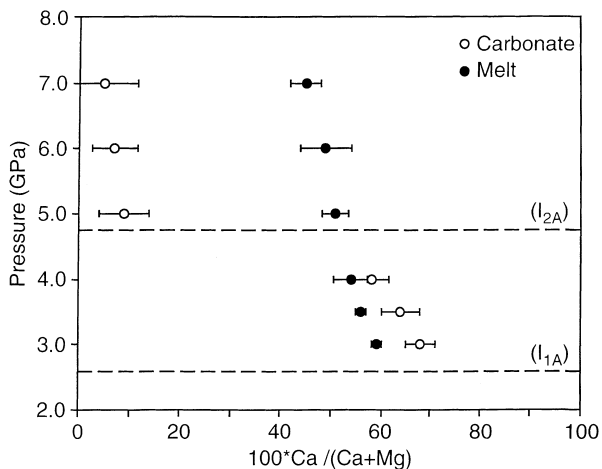


Fig. 6 Plot of pressure (GPa) against the Ca/(Ca + Mg) ratio of coexisting crystalline carbonate (*open circles*) and carbonate melt (*filled circles*). Data are taken from Table 3. The *dashed lines* represent the location of the invariant points $I_{1A}$ and $I_{2A}$ on the $CMAS.CO_2$ solidus (Fig. 4)

broad beam (15 µm) analysis of interstitial liquid in experiment KM48 (3 GPa) gives a Ca# of 0.64 and an $SiO_2$ content of 1.62 wt%. Thus, the value of 0.68 reported by Dalton and Wood (1993b) is attributed to quench modification of the interstitial melt that they analyzed. In Table 3 we report only analyses of the separated liquid.

From an analysis of phase relations in the $CMS.CO_2$ system at pressures just above $I_1$, Wyllie and Huang (1975, 1976) concluded that the first liquid produced by partial melting of an assemblage of forsterite + diopside + enstatite + carbonate would have a composition strongly influenced by the position of the temperature minimum on the liquidus for the $CaCO_3$-$MgCO_3$ system (see Fig. 9 of Wyllie and Huang 1976). Irving and Wyllie (1975) determined phase relations for the $CaCO_3$-$MgCO_3$ system at 3 GPa and reported a temperature minimum ($T_m$) at ~1290 °C for a composition near 58 mol% $CaCO_3$ (i.e. Ca# 0.58). Our data for the $CMAS.CO_2$ system at 3 GPa with a liquid composition of Ca# 0.59 are in agreement with the observations of Wyllie and Huang (1975, 1976) and demonstrate that the addition of $Al_2O_3$ does not greatly alter the liquidus relationships in $CMS.CO_2$ as was indicated by experiments on the join grossularite-calcite at 3 GPa (Maaløe and Wyllie 1975). Although there are as yet no data available for the $CaCO_3$-$MgCO_3$ system at pressures above 3 GPa, it is likely that the movement of $T_m$ towards $MgCO_3$ discovered by Byrnes and Wyllie (1981) in the pressure interval 1–3 GPa continues at high pressures. If so, the correlation between the Ca# of the temperature minimum in the $CaCO_3$-$MgCO_3$ system and the Ca# of carbonatitic melts in equilibrium with model lherzolite in both $CMS.CO_2$ and $CMAS.CO_2$ must extend to at least 7 GPa. This explains our observation that at pressures $>I_{2A}$, an Mg-rich carbonate (magnesite) coexists with a carbonate liquid of much lower Mg content. Figure 6 also shows that in the dolomite field, the Ca# of the melt is lower than the Ca# of the coexisting carbonate whereas the opposite is true for experiments in the magnesite stability field. This would be expected if, as discussed above, the melt composition is strongly influenced by the composition of $T_m$, as a carbonate on the Mg-rich side of $T_m$ (magnesite) will coexist with a less Mg-rich melt while the converse is true for a carbonate (magnesian calcite) on the Ca-rich side of $T_m$.

## Comparison with experimental data on natural compositions

In other experimental studies on carbonated peridotite in natural systems, Thibault et al. (1992) equilibrated carbonate melt with phlogopite lherzolite at 3 GPa and 1100 °C while Sweeney (1994) equilibrated carbonate melt with phlogopite-bearing, garnet clinopyroxenite at 3.4 GPa, also at 1100 °C. The Ca# of these melts are 0.51 and 0.53 respectively, in contrast to the more Ca-rich melts found in this study. However, a direct comparison of our data to these studies is not realistic as they were all conducted on Na and/or K-rich bulk compositions in the presence of water, all of which have a significant effect on the phase relations. Lee and Wyllie (1997) suggested that with alkalis present in the bulk composition, the Ca# in the melt decreases, an effect that is consistent with the differences between $CMAS.CO_2$, natural depleted lherzolite (Dalton and Wood 1993b) and the data of Thibault et al. (1992) and Sweeney (1994). Bulk composition, including volatiles, has a strong effect on the solidus and near-solidus carbonate melt composition, and primary carbonate melts will vary in, among other things, Ca# and alkali content, as discussed by Dalton and Wood (1993b).

## Concerning carbonatites

The experimental demonstration from this study and others that carbonate melt is in equilibrium with lherzolite under upper mantle conditions begs the question of the relationships between such melts and natural carbonatites found at the Earth's surface. It is not the purpose of this study to discuss at length the many debates surrounding carbonatite petrogenesis but our data do allow us to make a few observations.

The majority of carbonatites of both the intrusive and extrusive variety are calcitic with higher Ca# than those generated in high pressure experiments, i.e. the average Ca# of natural intrusive calciocarbonatites compiled by Woolley and Kempe (1989) is 0.95 compared to a Ca# of 0.59 for carbonate melt in equilibrium with garnet lherzolite at 3 GPa (Fig. 6). Thus, the experimental melts at pressures at and above $I_{1A}$ are much closer in composition to natural magnesiocarbonatites, the intrusive variety of which has an average Ca# of 0.59 (Woolley and Kempe 1989). An intriguing possibility, therefore, is that some magnesiocarbonatites represent direct eruption of carbonate melt from the mantle source region in a manner similar to kimberlite emplacement. Bailey (1989) described magnesiocarbonatite pyroclastic deposits from Rufunsa, Zambia, that carry melt droplets of high Sr, high Mn, Fe-free dolomite (Ca# 0.5–0.52) containing microphenocrysts of magnesiochromite that are compositionally equivalent to those found in mantle xenoliths in kimberlites. There are no associated silicate magmas at Rufunsa and the volcanological features are indicative of high-velocity diatremic eruption. These facts led Bailey (1989) to suggest that the Rufunsa volcanics were of direct mantle origin with the style of activity resembling that displayed by kimberlites. Our data are consistent with Bailey's suggestion, and a comparison of the Ca# of carbonate melts determined in this study (Table 3; Fig. 6) and that of the Rufunsa magnesiocarbonatites suggests generation from pressures of at least 3 GPa.

Any reasonable path of ascent of the Rufunsa carbonatite from its mantle source to the surface would cross the prominent solidus ledge shown in Figs. 1 and 4, which could cause crystallization and decarbonation, thereby preventing ascent. The ledge on the lherzolite-$CO_2$ solidus shown in Fig. 4 is represented by the reaction:

$$Olivine + Cpx + Garnet + CO_2 = Opx + Liquid. \quad (3)$$
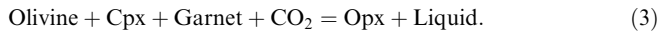
Carbonate (as melt or solid) is unstable in the presence of lherzolite at pressures below reaction (3). Consequently, a carbonatitic melt in equilibrium with lherzolite will crystallize and decarbonate on encountering the ledge as pressure decreases. However, this assumes that the ascending melt is in equilibrium with the peridotite wall-rock, which may not be the case (Wyllie 1980; Eggler 1987b). Given the low viscosity of carbonatitic melt (Janz et al. 1979), calculated eruption speeds of $CO_2$-rich melts from the upper mantle of 90 km/h$^{-1}$ (McGetchin and Ullrich 1973), and the diatremic style of eruption at Rufunsa, it is not unreasonable to suggest that this volcanic magnesiocarbonatite may well be an example of the eruption of carbonatitic melt directly from the mantle source that was out of equilibrium with the wall-rock through which it ascended. The possibility exists that other magnesiocarbonatites may have been generated in a similar manner.

## Low degree melts from peridotite – silica-rich or silica-poor?

There has been much controversy over the composition of low degree partial melts of peridotite, highlighted recently by the experiments of Baker et al. (1995) at 1 GPa, which suggest that near-solidus melts from fertile peridotite are enriched in $SiO_2$ (up to 57 wt%), $Al_2O_3$ and $Na_2O$. As pointed out by Kinzler and Langmuir (1995), the data of Baker et al. (1995) are at odds with natural data from alkaline rocks of both oceanic and continental settings, which indicate low $SiO_2$ contents for near-solidus melts and that the discrepancy could result from the fact that the experiments of Baker et al. (1995) were volatile-absent. From our data in CMAS-$CO_2$ from 3 to 7 GPa, it is evident that $CO_2$ has a dramatic effect on the melting behavior of lherzolite. At pressures greater than reaction (1A), even the smallest amount of $CO_2$ present in the mantle is stored in a carbonate mineral (Fig. 4) given appropriate conditions of mantle oxygen fugacity (Dalton and Wood 1995). Therefore, initial liquids from a lherzolite containing any amount of carbonate will be produced at the carbonated lherzolite solidus. In the presence of $H_2O$, melting will occur at lower temperatures than the model lherzolite-$CO_2$ solidus shown in Fig. 4 (White and Wyllie 1992). Although alkali content and Ca/Mg ratio of the solidus and near-solidus melt are dependent on bulk composition, these melts will be $CO_2$-rich and very poor in $SiO_2$ and $Al_2O_3$ (Table 3), quite the opposite to

the results for melting of volatile-absent lherzolite. That this situation exists in the mantle is demonstrated by the presence of $CO_2$-rich fluids in mid-ocean ridge basalts (Moore et al. 1977; Delaney et al. 1978; Kingsley and Schilling 1995), $CO_2$ inclusions in mantle xenoliths (Roedder 1965, 1984; Green and Radcliffe 1975; Rosenbaum et al. 1996), and the widespread occurrence of mantle xenoliths showing evidence of interaction with carbonatitic melts (Yaxley et al. 1991; Dautria et al. 1992; Hauri et al. 1993; Ionov et al. 1993; Rudnick et al. 1993). The rarity of carbonatites themselves at the Earth's surface most likely reflects lithospheric conditions rather than an absence of these magmas in the mantle source regions(s), and is supported by the repetition of carbonatite magmatism in specific areas over long periods of geological time (Barker 1996). These observations imply that low-degree carbonatitic melts are widely and readily available, with due consequences for mantle metasomatism and magmatism.

## References

Albee AL, Ray L (1970) Correction factors for electron-probe microanalysis of silicates, oxides, carbonates, and sulphates. Anal Chem 42: 1408–1414
Bailey DK (1989) Carbonate melt from the mantle in the volcanoes of south-east Zambia. Nature 388: 415–418
Bailey DK (1993) Carbonate magmas. J Geol Soc London 150: 637–651
Baker MB, Hirschmann MM, Ghiorso MS, Stolper EM (1995) Compositions of near-solidus peridotitic melts from experiments and thermodynamic calculations. Nature 375: 308–311
Barker DS (1996) Consequences of recycled carbon in carbonatites. Can Mineral 34: 373–387
Brenan JM, Watson EB (1991) Partitioning of trace elements between carbonate melt and clinopyroxene and olivine at mantle *P-T* conditions. Geochim Cosmochim Acta 55: 2203–2214
Brey GP, Brice WR, Ellis DJ, Green DH, Harris KL, Ryabchikov ID (1983) Pyroxene-carbonate reactions in the upper mantle. Earth Planet Sci Lett 62: 63–74
Byrnes AP, Wyllie PJ (1981) Subsolidus and melting relations for the join $CaCO_3$-$MgCO_3$ at 10 kbar. Geochim Cosmochim Acta 45: 321–328
Canil D, Scarfe CM (1990) Phase relations in peridotite + $CO_2$ systems to 12 GPa: implications for the origin of kimberlite and carbonate stability in the Earth's upper mantle. J Geophys Res 95, B10: 15805–15816
Dalton JA, Presnall DC (1997) No liquid immiscibility in the system $MgSiO_3$-$SiO_2$ at 5.0 GPa. Geochim Cosmochim Acta 61: 2367–2373
Dalton JA, Wood BJ (1993a) The partitioning of Fe and Mg between olivine and carbonate and the stability of carbonate under upper mantle conditions. Contrib Mineral Petrol 114: 501–509
Dalton JA, Wood BJ (1993b) The compositions of primary carbonate melts and their evolution through wallrock reaction in the mantle. Earth Planet Sci Lett 119: 511–525

Dalton JA, Wood BJ (1995) The stability of carbonate under upper-mantle conditions as a function of temperature and oxygen fugacity. Eur J Mineral 7: 883–891

Dautria JM, Dupuy C, Takherist D, Dostal J (1992) Carbonate metasomatism in the lithospheric mantle: peridotitic xenoliths from a melilititic district of the Sahara basin. Contrib Mineral Petrol 111: 37–52

Delaney JR, Muenow DW, Graham DG (1978) Abundance and distribution of water, carbon and sulfur in the glassy rims of submarine pillow basalts. Geochim Cosmochim Acta 42: 581–594

Eggler DH (1978) The effect of $CO_2$ upon partial melting of peridotite in the system $Na_2O$-CaO-$Al_2O_3$-MgO-$SiO_2$-$CO_2$ to 35 kb, with an analysis of melting in a peridotite-$H_2O$-$CO_2$ system. Am J Sci 278: 305–343

Eggler DH (1987a) Discussion of recent papers on carbonated peridotite, bearing on mantle metasomatism and magmatism: final comment. Earth Planet Sci Lett 82: 403

Eggler DH (1987b) Discussion of recent papers on carbonated peridotite, bearing on mantle metasomatism and magmatism: an alternative. Earth Planet Sci Lett 82: 398–400

Eggler DH, Wendlandt RF (1979) Experimental studies on the relationship between kimberlite magmas and partial melting of peridotite. In: Boyd FR, Meyer HOA (eds) Kimberlites, diatremes and diamonds: their geology, petrology, and geochemistry. Am Geophys Union, Washington DC, pp 330–338

Falloon TJ, Green DH (1989) The solidus of carbonated, fertile peridotite. Earth Planet Sci Lett 94: 364–370

Girnis AV, Brey GP, Ryabchikov ID (1995) Origin of Group 1A kimberlites: fluid-saturated melting experiments at 45–55 kbar. Earth Planet Sci Lett 134: 283–296

Green HW, Radcliffe SV (1975) Fluid precipitates in rocks from the Earth's mantle. Geol Soc Am Bull 86: 846–852

Gudfinnsson GH, Presnall DC (1996) Melting relations of model lherzolite in the system CaO-MgO-$Al_2O_3$-$SiO_2$ at 2.4–3.4 GPa and the generation of komatiites. J Geophys Res 101, B12: 27701–27709

Haggerty SE (1994) Superkimberlites: a geodynamic diamond window to the Earth's core. Earth Planet Sci Lett 122: 57–69

Haggerty SE, Sautter V (1990) Ultra-deep (> 300 km), ultramafic, upper mantle xenoliths. Science 248: 993–996

Hauri EH, Shimizu N, Dieu JJ, Hart SR (1993) Evidence for hotspot-related carbonatite metasomatism in the oceanic upper mantle. Nature 365: 221–227

Herzberg C, Gasparik T, Sawamoto H (1990) Origin of mantle peridotite: constraints from melting experiments to 16.5 GPa. J Geophys Res 95, B10: 15779–15803

Ionov DA, Dupuy C, O'Reilly SY, Koplova MG, Genshaft Y (1993) Carbonated peridotite xenoliths from Spitsbergen: implications for trace element signature of mantle carbonate metasomatism. Earth Planet Sci Lett 119: 283–297

Ionov DA, O'Reilly SY, Genshaft Y, Koplova MG (1996) Carbonate-bearing mantle peridotite xenoliths from Spitsbergen: phase relationships, mineral compositions and trace element residence. Contrib Mineral Petrol 125: 375–392

Irving AJ, Wyllie PJ (1975) Subsolidus and melting relationships for calcite, magnesite and the join $CaCO_3$-$MgCO_3$ to 36 kb. Geochim Cosmochim Acta 39: 35–53

Janz GJ, Allen CB, Bansal NP, Murphy RM, Tomkins RPT (1979) Physical properties data compilations relevant to energy storage. II. Molten salts: data on single and multi-component systems. Nat Stand Ref Data Ser NSRSDS-NBS 61, part II. US Nat Bur Stand

Katsura T, Ito E (1990) Melting and subsolidus phase relations in the $MgSiO_3$-$MgCO_3$ system at high pressures: implications to evolution of the Earth's atmosphere. Earth Planet Sci Lett 99: 110–117

Kingsley RH, Schilling J-G (1995) Carbon in Mid-Atlantic Ridge basalt glasses from 28°N to 63°N: evidence for a carbon-enriched Azores mantle plume. Earth Planet Sci Lett 129: 31–53

Kinzler RJ, Langmuir CH (1995) Minute mantle melts. Nature 375: 274–275

Lane SJ, Dalton JA (1994) Electron microprobe analysis of geological carbonates. Am Mineral 79: 745–749

Lee W-J, Wyllie PJ (1994) Experimental data bearing on liquid immiscibility, crystal fractionation, and the origin of calciocarbonatites and natrocarbonatites. Int Geol Rev 36: 797–819

Lee W-J, Wyllie PJ (1997) Liquid immiscibility between nephelinite and carbonatite from 1.0 to 2.5 GPa compared with mantle melt compositions. Contrib Mineral Petrol 127: 1–16

Lee W-J, Wyllie PJ, Rossman GR (1994) $CO_2$-rich glass, round calcite crystals, and no liquid immiscibility in the system CaO-$SiO_2$-$CO_2$ at 2.5 GPa. Am Mineral 79: 1135–1144

Maaløe S, Wyllie PJ (1975) The join grossularite-calcite through the system CaO-$Al_2O_3$-$SiO_2$-$CO_2$ at 30 kilobars: crystallization range of silicates and carbonates on the liquidus. Earth Planet Sci Lett 28: 205–208

McGetchin TR, Ullrich GW (1973) Xenoliths in maars and diatremes with inferences for the Moon, Mars, and Venus. J Geophys Res 78: 1833–1853

Moore JG, Batchelder JN, Cunningham CG (1977) $CO_2$-filled vesicles in mid-ocean ridge basalt. J Volcanol Geotherm Res 2: 309–327

Moore RO, Gurney JJ (1985) Pyroxene solid solution in garnets included in diamonds. Nature 318: 553–555

Mysen BO (1975) Solubility of volatiles in silicate melts at high pressure and temperature: the role of carbon dioxide and water in feldspar, pyroxene, and feldspathoid melts. Carnegie Inst Washington Yearb 74: 454–468

Presnall DC (1986) An algebraic method for determining equilibrium crystallization and fusion paths in multicomponent systems. Am Mineral 71: 1061–1070

Ringwood AE, Kesson SE, Hibberson W, Ware N (1992) Origin of kimberlites and related magmas. Earth Planet Sci Lett 113: 521–538

Roedder E (1965) Liquid $CO_2$ inclusions in olivine-bearing nodules and phenocrysts from basalts. Am Mineral 50: 1746–1782

Roedder E (1984) Fluid inclusions (Reviews in Mineralogy vol. 12). Mineralogical Society of America, Washington DC

Rosenbaum JM, Zindler A, Rubenstone JL (1996) Mantle fluids: evidence from fluid inclusions. Geochim Cosmochim Acta 60: 3229–3252

Rudnick RL, McDonough WF, Chappel BW (1993) Carbonatite metasomatism in the northern Tanzanian mantle: petrographic and geochemical characteristics. Earth Planet Sci Lett 114: 463–475

Sautter V, Haggerty SE, Field S (1991) Ultra-deep (> 300 km), ultramafic xenoliths: new petrological evidence from the transition zone. Science 252: 827–830

Sweeney RJ (1994) Carbonatite melt compositions in the Earth's mantle. Earth Planet Sci Lett 128: 259–270

Thibault Y, Edgar AD, Lloyd FE (1992) Experimental investigation of melts from a carbonated phlogopite lherzolite: implications for metasomatism in the continental lithospheric mantle. Am Mineral 77: 784–794

Wallace ME, Green DH (1988) Experimental determination of primary carbonatite magma composition. Nature 335: 343–346

Watson EB (1979) Calcium content of forsterite coexisting with silicate liquid in the system $Na_2O$-CaO-MgO-$Al_2O_3$-$SiO_2$. Am Mineral 64: 824–829

White BS, Wyllie PJ (1992) Solidus reactions in synthetic lherzolite-$H_2O$-$CO_2$ from 20–30 kbar, with applications to melting and metasomatism. J Volcanol Geotherm Res 50: 117–130

Woolley AR, Kempe DRC (1989) Carbonatites: nomenclature, average chemical compositions, and element distribution. In: Bell K (ed) Carbonatites: genesis and evolution. Unwin Hyman, London, pp 1–14

Wyllie PJ (1977) Mantle fluid compositions buffered by carbonates in peridotite-$CO_2$-$H_2O$. J Geol 85: 187–207

Wyllie PJ (1980) The origin of kimberlite. J Geophys Res 85, B12: 6902–6910

Wyllie PJ, Huang W-L (1975) Peridotite, kimberlite, and carbonatite explained in the system CaO-MgO-$SiO_2$-$CO_2$. Geology 3: 621–624

Wyllie PJ, Huang W-L (1976) Carbonation and melting reactions in the system CaO-MgO-SiO$_2$-CO$_2$ at mantle pressures with geophysical and petrological applications. Contrib Mineral Petrol 54: 79–107

Wyllie PJ, Huang W-L, Otto J, Byrnes AP (1983) Carbonation of peridotites and decarbonation of siliceous dolomites repre-sented in the system CaO-MgO-SiO$_2$-CO$_2$ to 30 kbar. Tectonophysics 100: 359–388

Yaxley GM, Crawford AJ, Green DH (1991) Evidence for carbonatite metasomatism in spinel peridotite xenoliths from western Victoria, Australia. Earth Planet Sci Lett 107: 305–317